Available online at www.sciencedirect.com

jmr&t Journal of Materials Research and Technology

journal homepage: www.elsevier.com/locate/jmrt

Original Article

Augmentation of weld penetration by flux assisted TIG welding and its distinct variants for oxygen free copper

Harikrishna Rana [a], *Vishvesh Badheka* [b], *Parth Patel* [a], *Vivek Patel* [c,d,*], *Wenya Li* [d], *Joel Andersson* [c]

[a] *LDRP Institute of Technology & Research, KSV University, Gandhinagar, Gujarat, India*
[b] *Pandit Deendayal Petroleum University, Raisan, Gandhinagar, Gujarat, India*
[c] *Department of Engineering Science, University West, Trollhättan, 46186, Sweden*
[d] *School of Materials Science and Engineering, Northwestern Polytechnical University, Xi'an, 710072, Shaanxi, PR China*

ARTICLE INFO

Article history:
Received 11 November 2020
Accepted 4 December 2020
Available online 9 December 2020

Keywords:
A-TIG
FZ-TIG Welding
Flux
Oxide
Weld penetration
Copper

ABSTRACT

A comparative study to investigate the influences of single component fluxes on the depth-to-width ratio (DWR) of oxygen free copper was carried out with novel variants of tungsten inert gas (TIG) welding namely Activated TIG (A-TIG), Flux Bounded TIG (FB-TIG) and Flux Zoned TIG (FB-TIG) processes. The experiments to identify the fluxes delivering the higher DWRs in A-TIG welding among thirteen distinct fluxes were followed by the trials with FB-TIG and FZ-TIG employing those identified DWR fluxes. The fluxes which outperformed with all the techniques were MoO_3 & MgO. Reversed Marangoni and arc constriction mechanisms were perceived to be opt for such an increase in DWR. Metallurgical characterization of the weldment indicated distinct grain morphologies and certain defects as well in the weld zones. The FZ-TIG welding is postulated to surpass all the techniques in terms of bringing about the upmost weld penetration.

1. Introduction

A-TIG welding is an innovative variant of TIG welding, invented at Paton institute of electric welding in the 1960's [1]. Initially, activating flux coating (viz., oxides and halides) is applied on the whole weld area of prepared parent metal, followed by TIG welding as indicated in Fig. 1(a). These majorly non-conductive fluxes resist the current and lead to arc constriction which evidently increases the current density and the arc forces while welding. As the flux decomposes and dissolves in molten metal with the tremendous arc force the weld pool penetration may raise up to 300% as compared to conventional TIG welding [2,3]. A-TIG welding has been reportedly successful in getting higher depth of penetration (DOP) for various materials including carbon steel [4], titanium

* Corresponding author.
E-mail address: vivek.patel@hv.se (V. Patel).
https://doi.org/10.1016/j.jmrt.2020.12.009

alloys [5,6], stainless steels [7,8], etc. Furthermore, variants like FB-TIG and FZ-TIG welding has also been developed and experimented [9–12] by altering the geometrical placement of fluxes. In the FB-TIG welding, two strips of flux is coated on either sides of the center weld line leaving a small gap at the center of the plate as indicated in Fig. 1(b) whereas in the FZ-TIG welding, a flux coat comprising high melting point, high boiling point and low electrical conductivity and another flux coat with low melting point, low boiling point and high electrical conductivity are applied on the side and central regions of the weld surface respectively as displayed in Fig. 1(c).

By means of A-TIG welding, various processing conditions such as single component flux/mixture of fluxes, current, voltage, torch travelling speed etc., have been studied and their effects on the weld bead dimensions, microstructure and mechanical properties have been reported in the majority of investigations [13,14]. Vora et al. [15] have experimented with different single component fluxes viz., CaO, Fe_2O_3, MnO_2, TiO_2, and ZnO etc., on the 6 mm thick LAFM steel substrate and reported full weld bead penetration using Fe_2O_3 flux. A rise in the DOP was reportedly attributed to different mechanisms like reversed Marangoni and arc constriction. Reverse Marangoni effect was reportedly evident with CaO, Fe_2O_3, MnO_2, TiO_2 and ZnO fluxes while arc constriction effect for Fe_2O_3 and TiO_2 fluxes. Ramkumar et al. [16] reported full weld penetration in 5 mm thick Inconel 718 alloy substrate using SiO_2 and TiO_2 fluxes at 140 A current. Authors also confirmed average fusion zone (FZ) hardness greater than BM hardness employing both fluxes. Dhandha et al. [17] have also reported full penetration welding of 6 mm thick P91 steel plate using TiO_2 flux employing single pass of A-TIG welding. Kumar et al. [18] have experimented with two different fluxes viz., SiO_2 and ZnO on the Incoloy 800H substrate, and reported a 16% rise in DOP for SiO_2 flux and considerable increase in the section hardness for both fluxes. Nayee et al. [2] have also succeeded to weld 6 mm thick dissimilar substrate materials viz., carbon steel to stainless steel employing A-TIG technique with TiO_2 flux. As compared to unaided TIG welding trials the higher joint efficiency and lower angular distortion were reported in A-TIG experiments. Moreover, several investigations have also been reported the use of hybrid (a mixture of two or more) fluxes with the aim of increasing DOP. Li et al. [19] succeeded to increase the DWR by 118% using flux mixture (70% TiO_2 + 30% CaF_2) and reported 89% rise in the ultimate tensile strength (UTS) of the joint as compared to normal TIG welded samples. Lin et al. [10] achieved full plate penetration using 50% SiO_2 + 50% MoO_3 flux for 6.35 mm thick Inconel 718 alloy plate.

On the other hand, FB-TIG and FZ-TIG, (variants of A-TIG welding) have also been studied in the context of improving the DWR and overall weld properties. Babu et al. [20,21] investigated that FB-TIG welding of AA 2219-T87 aluminium alloy using SiO_2 flux produced aesthetically superior and liquidation crack free weld region as compared to conventional TIG methods. In addition, UTS and yield strength of weld region was improved by 50–54% evidently. A study of FB-TIG carried by Jaykrishnan et al. [22] on commercially pure aluminium using different particle size of activating fluxes like SiO_2, TiO_2, Al_2O_3, Fe_2O_3 and Cr_2O_3 indicated that small particle size flux increases penetration by 303% than large particle flux. Also, the flux gap plays a very crucial role to achieve high DOP. When the flux gap was kept in range of 4–5 mm the DOP was boosted by at least 5 times compared to conventional TIG welding [23]. However, as per the claims raised by Huang et al. [11] FZ-TIG is the superior and most advanced technique which reportedly conglomerates the positives of both A-TIG and FB-TIG variants of TIG welding.

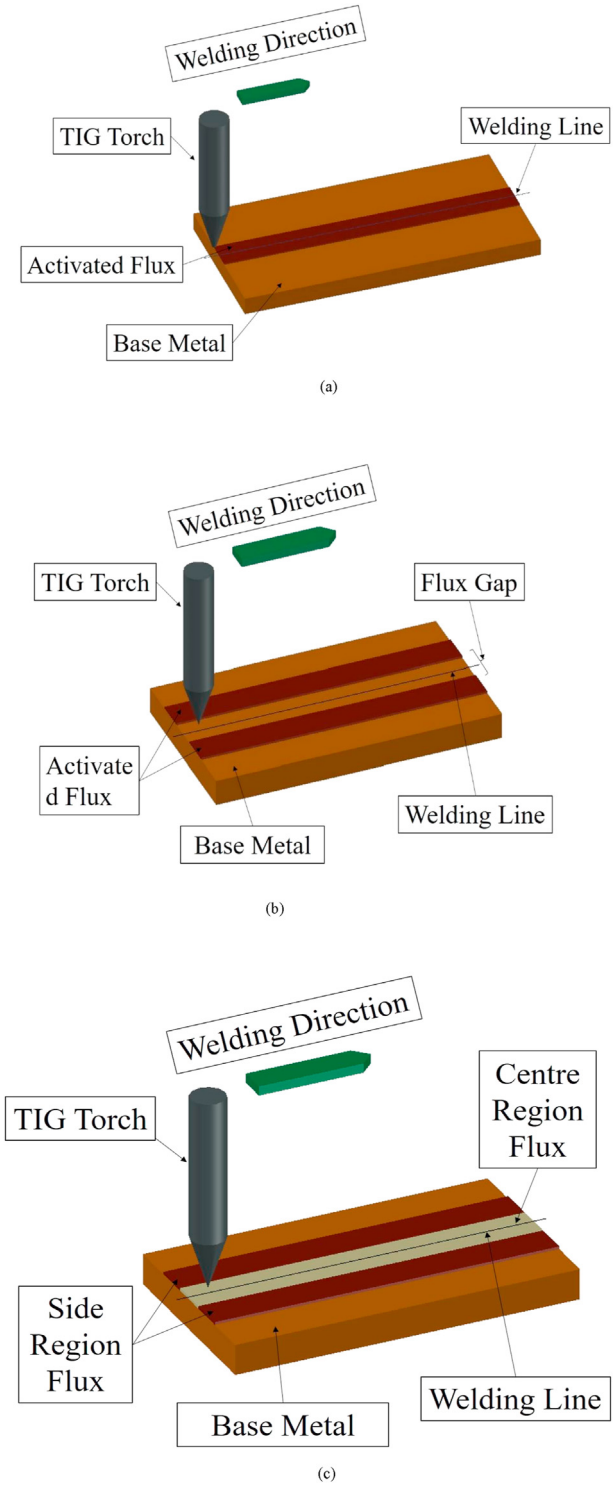

Fig. 1 – Schematic diagram of variants of activated flux assisted TIG welding: (a) A-TIG (b) FB-TIG (c) FZ-TIG.

Table 1 – Physical characteristics of fluxes [53].

IUPAC name of flux	Molecular formula	Density (ρ) (gram/cm^3)	Melting Temp. (°C)	Weight (gram)
Zinc oxide	ZnO	5.61	1975 (decompose)	0.33
Calcium oxide	CaO	3.35	2613	0.22
Manganese (IV) oxide	MnO_2	5.03	535 (decompose)	0.3
Silicon dioxide	SiO_2	2.65	1713	0.185
Chromium (VI) oxide	CrO_3	2.7	197	0.18
Copper (II) oxide	CuO	6.31	1326	0.365
Molybdenum (VI) oxide	MoO_3	4.69	795	0.285
Cobalt (II, III) oxide	Co_3O_4	6.11	895	0.355
Magnesium oxide	MgO	3.58	2825	0.23
Nickel (II) oxide	NiO	6.67	1955 (decompose)	0.385
Mercury (II) oxide	HgO	11.14	500 (decompose)	0.6
Magnesium dichloride hexahydrate	$MgCl_2*6H_2O$	1.569	118, 100 (decompose)	0.13
Calcium difluoride	CaF_2	3.18	1418	0.21

Huang et al. [11] applied this novel technique on aluminium A3003 alloy using custom made FZ108 flux which contained mixture of several halides and elementary substances as centre region flux while SiO_2 selected as side region flux. The results surprisingly indicated that DOP achieved by FZ-TIG was more than three times that of the conventional TIG and almost twice that of A-TIG welding. Young et al. [24] has also reported threefold increase in the DOP as compared to conventional TIG welding with noticeable increase in the mechanical properties in the Aluminium alloy.

Another important non-ferrous metal copper which is extensively used in heat exchangers, semiconductors, power generating equipment etc., due to its high thermal and electrical conductivity and unmatched corrosion resistance. Despite being known that GTAW of non-ferrous materials is difficult, several research investigations are available in GTAW of aluminum [21], magnesium [25] and Inconel metals and alloys [10,14,26]. However, very limited research has been reported in the field of TIG welding of copper and its alloy, owing to insufficient welding temperature caused by the higher thermal and electrical conductivity. This includes the work patented by Segletes et al. [27] who used hybrid fluxes in A-TIG technique for welding of 95–99% pure copper and reported full weld pool penetration in 5 mm thick copper sheet. Moreover, considerable work has been reported for solid state welding techniques like friction stir welding (FSW) for copper, aluminum and magnesium alloys, and their dissimilar combinations such as copper to titanium and copper to steel [28–31]. Inline, it is perceived to have great potential to work in the field of TIG welding and its variants for joining the copper plates. They seem to play the crucial role by using activated fluxes for increasing the heat input while welding and ultimately DOP of weld pool.

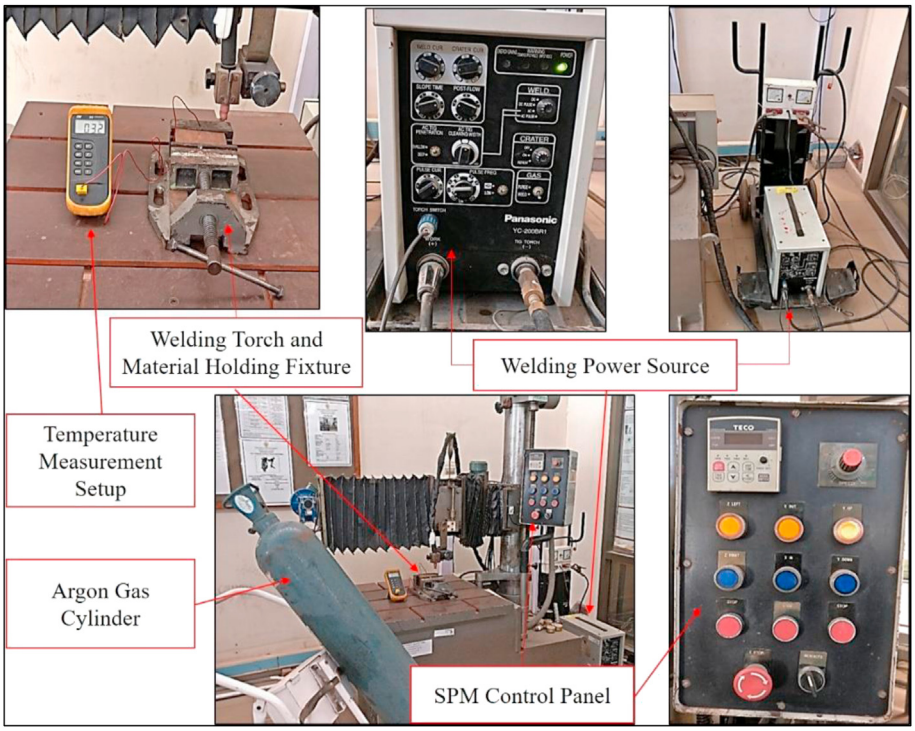

Fig. 2 – A-TIG welding setup.

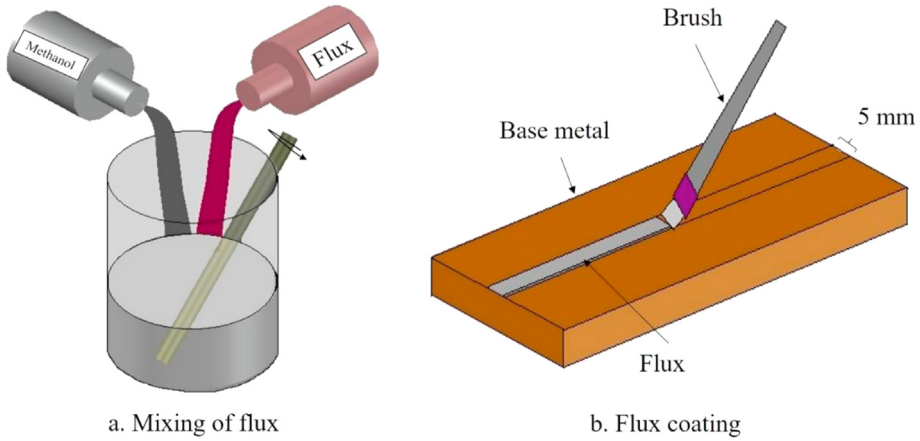

Fig. 3 – Preparation and application of flux coat.

2. Experimental procedure

2.1. Base metal

Oxygen-free copper (Cu - 99.99wt%, O – 10 ppm, impurities–0.01wt% max.) strips having dimensions: *l*:100 mm × *w*:30 mm × *t*:6 mm, were prepared for bead-on-plate study. They were roughly polished (top of the plate) with 120, 320 grit (SiC) flexible abrasive papers to remove surface impurities followed by cleaning of welding surface using methanol. All thirteen fluxes selected for A-TIG trials. The fluxes which stood in top four position were selected for FB-TIG welding. And for FZ-TIG welding MoO_3 and MgO selected for centre region flux while TiO_2, Fe_2O_3 and Al_2O_3 were selected for side region flux.

2.2. Fluxes

Initially A-TIG welding experiments were performed using thirteen different flux coats (Supplied by: M/s Merck Specialities Private Limited, Mumbai) as mentioned in Table 1 with their physical characteristics. Available powder form fluxes were converted to paste by mixing it with acetone and then applied on plate by using paint brush having width of 5 mm as shown in Fig. 3. Acetone having tendency to vaporize quickly leaving evenly distributed flux on the plate surface. Flux layer thickness approximately kept about 0.10 mm. To ensure uniform thickness the required quantities of fluxes were calculated as shown in Table 1 and entire amount of flux was pasted on the flux region. A-TIG experiments were followed by FB-TIG welding experiments using top four fluxes (MoO_3, MgO, SiO_2 and CaF_2) which delivered highest DWR. Finally, the FB-TIG experiments were performed with MoO_3 and MgO flux coats in the centre region and TiO_2, Fe_2O_3 and Al_2O_3 (with high resistivity) in the side region.

2.3. Experimental setup

All the experiments were carried out on a customized special purpose GTAW machine having independent torch movement in X, Y & Z axis. (Make: Panasonic, model: YC-200BR1 (AC/DC), 200 A). The substrate plates were held in the fixture and trails were undertaken with shielding of Argon gas as depicted in Fig. 2. Bead on plate welding trials was carried out to understand the effect of fluxes on weld morphology. OFC strips were prepared and cleaned using 120–320 mesh abrasive papers and acetone respectively before welding. However, the application area for each A-TIG variant was varied as described earlier (see Section 1). Autogenous TIG welding experiments were carried out on OFC plates to produce bead-on-plate welds using parameters mentioned in Table 2.

2.4. Metallographic study and measurement

Samples for the metallographic observations were sliced from the center of the weld bead. All the samples were polished down to 1 μm using standard microstructural procedure followed by etching (HnO_3: 5 ml, H_2SO_4: 5 ml, CrO_3: 4 gm, NH_4Cl: 1 gm and H_2O: 90 ml) [32]. Study of weld bead morphology and metallography were carried out using an Olympus SZ61 stereomicroscope which was followed by scanning electron microscopy (SEM) and energy despersive x-ray sprectroscopy (EDS) analysis for selective specimens.

3. Result and discussion

The phenomenon of increasing the weld bead penetration by means of activating fluxes is quite complex and hence a

Table 2 – Welding parameters.

Parameters	Value
Electrode type	2% Thoriated Tungsten
Electrode diameter	3.2 mm
Electrode tip angle	55–60°
Welding current	200 A
Crater current	200 A
Shielding gas	Pure Argon (99.999%)
Argon flow rate	15 lit/min
Torch angle	90°
Torch travel speed	55 mm/min
Arc gap	2 mm

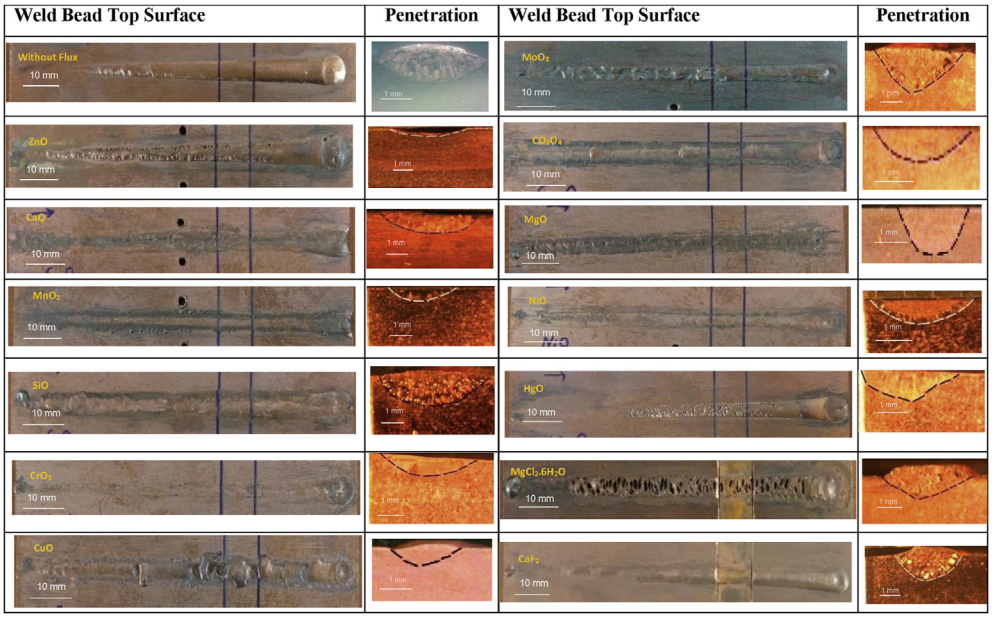

Fig. 4 – Weld appearance and macrostructures of samples prepared without and with different fluxes.

complete analysis for the same have been reported at a few instances. Those mechanisms are arc constriction mechanism [33,34], reversed Marangoni mechanism [17,35], electromagnetic forces mechanism [36], buoyancy and aerodynamic forces mechanism [37]. From the experimental results of the present investigation, it became clear that every flux is unique in their chemical, thermal and electrical properties which resulted in different weld bead dimensions, owing to one or more of the said mechanisms.

3.1. *Effect of fluxes on weld surface*

The macroscopic cross-sections of welding beads and resulting penetrations under the standard welding conditions without and with different fluxes are displayed in Fig. 4. On the one hand incessant linear spatter was evident on the top surface of A-TIG welded specimens using fluxes such as CaO, SiO_2, MoO_3, MgO, NiO etc. Such an excessive spatter with those fluxes may have been caused by strong arc constriction resulted from higher peak temperature while processing as mentioned in Table 3. During A-TIG welding the arc electrons movements are hindered by the deposited flux at the center as most of them are good insulators of electricity. As the electrons flow towards the least resistant path which is on the sideways resulting into the arc wandering and the spatter thereby. Hence, A-TIG welding produces more non-uniformities on the top surface of specimens as compared to TIG welding which are attributed to inevitable spatter generation by residual slag [38]. On the one the other hand less amount of spatter were evident in the case of CuO, HgO, CrO_3 fluxes, attributing to the slag layer formed by the flux deposited prior to the welding. However, the phenomenon is inversed in the case of FB-TIG welding as the center region stays uncoated and the side regions are coated instead. This leads to the more arc control and constriction to the center. Therefore, comparatively lesser amount of spatter was observed in those FB TIG welding samples as displayed in Fig. 5. Moreover, each set of FZ-TIG experiments have shown considerable spatter on weld surface which are attributable to the strong arc constriction and arc force (see Fig. 6).

3.2. *Effect of fluxes on arc characteristics, heat input, and peak temperatures*

Amount heat flux generated while welding largely relies on the arc voltage and current while welding [39]. The heat flux and arc parameters can be related to the following equation [40].

$$Q = \frac{\eta * VI}{\pi R^2} \quad (1)$$

where, Q = Heat flux per unit area, η = Welding arc efficiency, V = Arc voltage, I = Current, R = Radius of the arc root.

As per the equation, the heat flux is directly proportional to the induced voltage. The arc gap majorly contributes to the arc voltage, which was kept invariable during all the experiments.

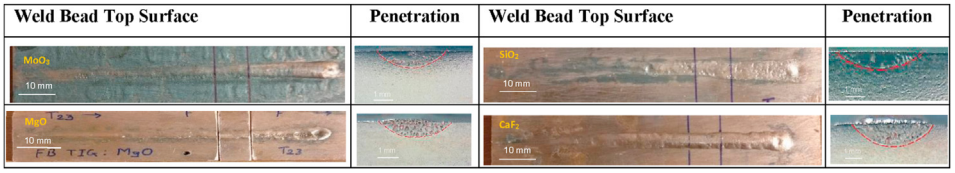

Fig. 5 – Weld appearance and macrostructures of FB – TIG welding specimens.

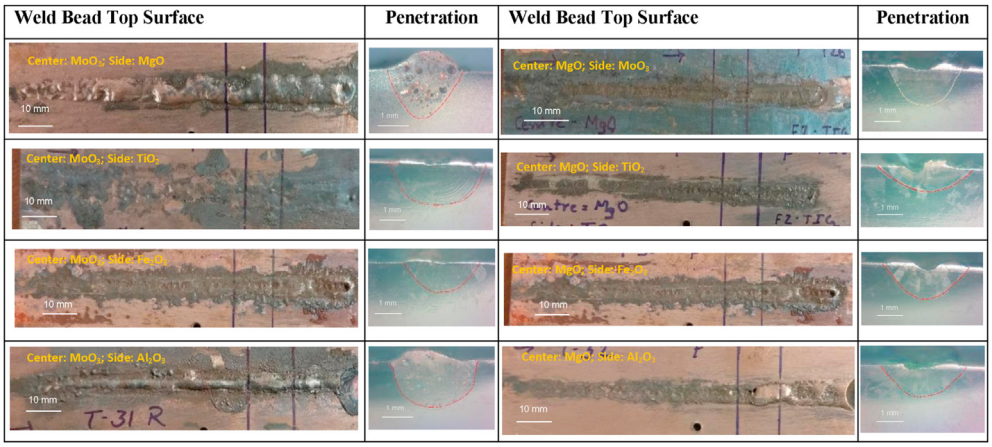

Fig. 6 – Weld appearance and macrostructures of FZ – TIG welding specimens.

However, the distinct ionization potential of various fluxes within the arc gap influences the arc behavior. In the case of the oxide fluxes, oxygen is disintegrated at elevated arc temperatures while welding, which thereby leads to variation in the resistance to the passage of electric current within the arc [41]. On account of the distinct physical properties of the different fluxes mentioned in Table 1, varied results of voltage were recorded as summarized in Table 3.

MoO_3 flux exhibited highest ~ 20% increase in the arc voltage as compared to normal TIG welding. During the A-TIG welding, physically constricting the plasma column reduces the conducting cross section of the arc channel. Consequently, to withstand uninterrupted arc current at the constant current set by welding equipment, arc voltage is required to be increased [42]. Additionally, the electronegativity of the flux components has been reported to play a pivotal role in the arc characteristics and the heat generated thereby. In the course of the A-TIG & FZ-TIG welding disintegration of the oxide flux results into the separation of chemical element and oxygen. The properties of oxide can be described by the electronegativity of a particular chemical element in conjunction with the oxygen (E.g. Molybdenum for MoO_3). As the electronegativity of the Molybdenum is the highest among the distinct fluxes experimented, due to which oxygen atoms dissociated from MoO_3 captivates more electrons in the outer region of the arc column as compared to the

Table 3 – Voltage and peak temperature recorded with use of activating fluxes.

Welding Technique	Flux	Voltage (V)	Peak Temp. (°C)	DOP	D/W ratio	Reverse Marangoni Effect	Arc Constriction Mechanism
A-TIG	Normal TIG	14	658	0.857	0.198	Absent	Absent
	ZnO	15	770	0.561	0.149	Absent	Absent
	CaO	17	824	0.876	0.209	Absent	Absent
	MnO_2	13	561	0.65	0.271	Absent	Absent
	SiO_2	15.5	731	1.123	0.376	Present	Absent
	CrO_3	15	728	0.719	0.276	Absent	Present
	CuO	15	651	0.831	0.287	Absent	Present
	MoO_3	16.5	725	1.773	0.463	Present	Present
	Co_3O_4	13	623	0.562	0.238	Absent	Absent
	MgO	15.5	692	1.594	0.430	Present	Present
	NiO	15.5	917	0.786	0.278	Absent	Present
	HgO	14.5	662	0.629	0.212	Absent	Present
	$MgCl_2*6H_2O$	15	715	1.212	0.325	Present	Present
	CaF_2	14.5	642	1.30	0.333	Present	Present
FB-TIG	MoO_3	13.5	667	1.231	0.293	Present	Present
	MgO	17	758	1.496	0.371	Present	Present
	SiO_2	15.5	741	0.676	0.195	Absent	Absent
	CaF_2	17	706	1.183	0.283	Present	Present
FZ-TIG	Centre Side						
	MoO_3 MgO	15	761	3.883	0.603	Present	Present
	MoO_3 TiO_2	17.5	806	2.599	0.408	Present	Absent
	MoO_3 Fe_2O_3	16	603	1.393	0.288	Present	Absent
	MoO_3 Al_2O_3	19.5	914	3.818	0.642	Present	Present
	MgO MoO_3	15.5	668	2.023	0.454	Present	Present
	MgO TiO_2	16	818	1.152	0.258	Absent	Present
	MgO Fe_2O_3	16.5	611	1.622	0.335	Present	Present
	MgO Al_2O_3	17	801	2.036	0.377	Absent	Present

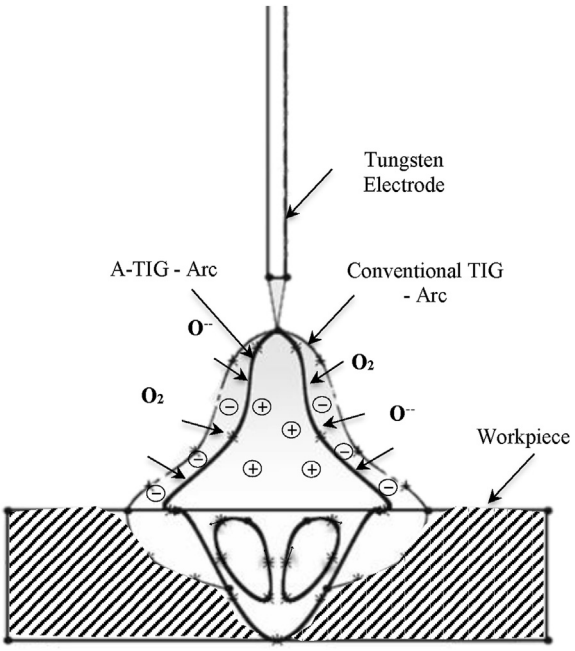

Fig. 7 – Arc Constriction by -Ve ion formation at the edge of the arc leading to increased current density at the centre of the anode.

rest [42]. The negative ions generated by the electron aggregation at the arc edge could result in to arc constriction. This constriction surges current density at the anode center instigating higher DOP subsequently. That is to say that the arc column made with MoO_3 flux exhibited greater constriction and resulting higher DOP as depicted in Fig. 7. Moreover, the MgO flux also exhibited the second highest temperature during experiments. This is attributed to the highest melting point among all the fluxes. Addition of the activating fluxes with high melting point at center of the weld induces the higher surface tension there as reported by the Keene et al. [43] The higher surface tension at the center and lower at the edges drives the molten weld metal flow towards the center instead of outwards as in the case of conventional TIG welding. This mechanism of inversed surface tension gradient leading to the narrow and deep penetration is termed as the Reverse Marangoni Convection effect as well explained in the publication made by Leconte et al. [44] Hence, it can be postulated that more than one mechanism are evident causing the increased weld penetration.

Nonetheless, the scenario is little varied with FB-TIG welding as the location of flux deposition is altered as discussed in Section 1. When the arc is initiated, apart from the center region it also interacts with the flux particles located on the side regions. The intense heat from the arc dissociates the flux particles leading to the vaporization and further vapour cloud formation besides the arc column. The interactions among the flux cloud particles and bordering electron with comparatively lower amount of energy than core region inhibits the arc broadening further. That is to say that with this narrow arc the higher DOP was apparent in some of the experiments as described in Table 3. However, FZ-TIG welding specimens have experienced the combination of the mechanism as discussed earlier as it is a combined approach which comprises of A-TIG welding and FB-TIG welding characteristics. Hence, those samples exhibited narrower weld bead with higher DOP as compared to both aforementioned approaches.

3.3. *Effect of fluxes on the weld bead dimensions*

Apart from the weld bead appearance, these fluxes majorly influenced weld bead dimensions as depicted in the chart (Fig. 8). As compared to normal TIG welding samples, almost all the samples processed with A-TIG exhibited a decline in the weld bead width (BW). Additionally, several samples displayed increased DOP as compared to normal TIG samples. The highest DOP and depth to width ratio (DWR) were

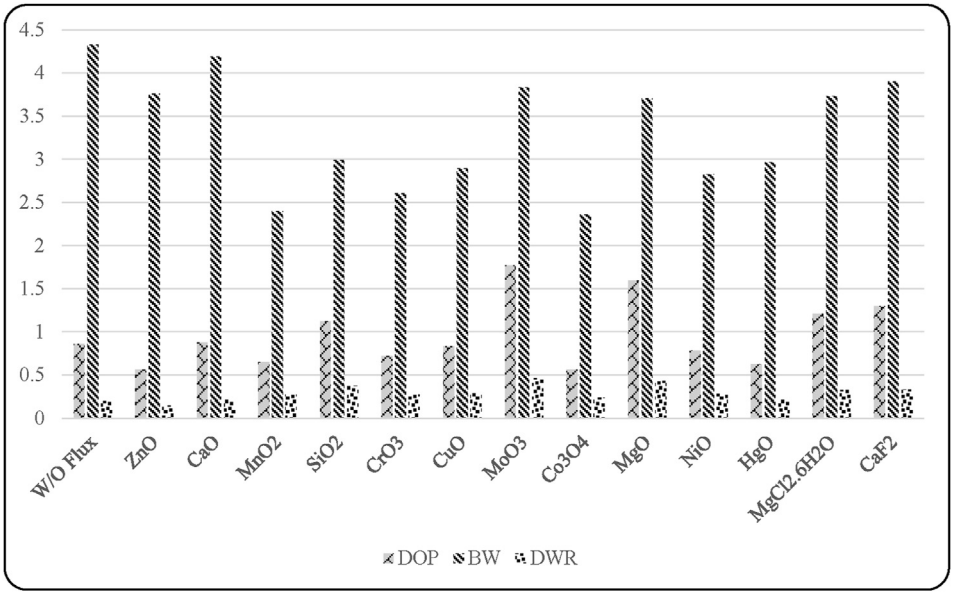

Fig. 8 – Comparison of DOP, BW and DWR of different A-TIG weld samples with normal TIG weld sample.

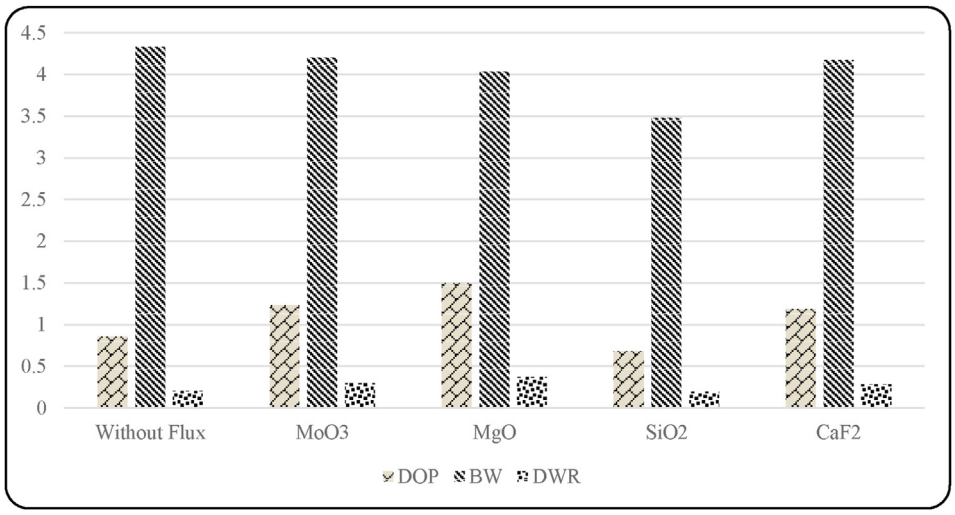

Fig. 9 – Comparison of DOP, BW and DWR of different FB-TIG weld samples with normal TIG weld sample.

witnessed with MoO_3 flux. Here, the higher DOP may be attributed to several phenomenon like (a) Flux chemical composition having higher oxygen content, which dissociates while welding and may lead to higher current density resulting in the higher DOP [45] (b) Higher arc voltage generated while welding which also may be the cause for increased DOP. The distinct properties such as thermal and electrical conductivity, electronegativity etc. of different fluxes majorly influence the arc characteristics (current, voltage, arc shape etc.) during welding [15]. (c) The heat input while welding also plays a significant role in the DOP. The fluxes having lower thermal conductivity offers higher resistance for dissolution/melting which leads to higher peak temperatures to others. However, in the present context, MoO_3 has not displayed the highest peak temperature. Though it is higher as compared to the no-flux samples and several other samples prepared with fluxes. As more than one cause might be prevailing for a higher DOP, it becomes difficult to decide on the percentage contributions of the individuals.

Various mechanisms such as reversed Marangoni convection, arc constriction, flux insulation effect etc. have been reported to be responsible for the change in the weld bead dimensions. There were several fluxes such as MoO_3, MgO, $MgCl_2.6H_2O$, SiO_2, and CaO, which clearly indicated the presence of the arc constriction. As per the mechanism, the flux deposited on the substrate acts as an insulation resistance to the arc current, which in turn increases the heat input at the center of the weld pool. The arc current and temperature at the center is required to be adequate for melting of the flux, which may further wipe out the flux with the arc force, then only the current may easily penetrate the substrate. As the fluxes are wiped out, the arc diameter at the weld pool surface is reduced by the insulating effect of these flux in the outer region. Consequently, the current density at the central region increases resulting in the increase in the magnetic pinch force generated by the arc and the pressure in the weld puddle. This led to the strong convective material flow downward in the weld puddle and thereby increases the DOP. However, as in

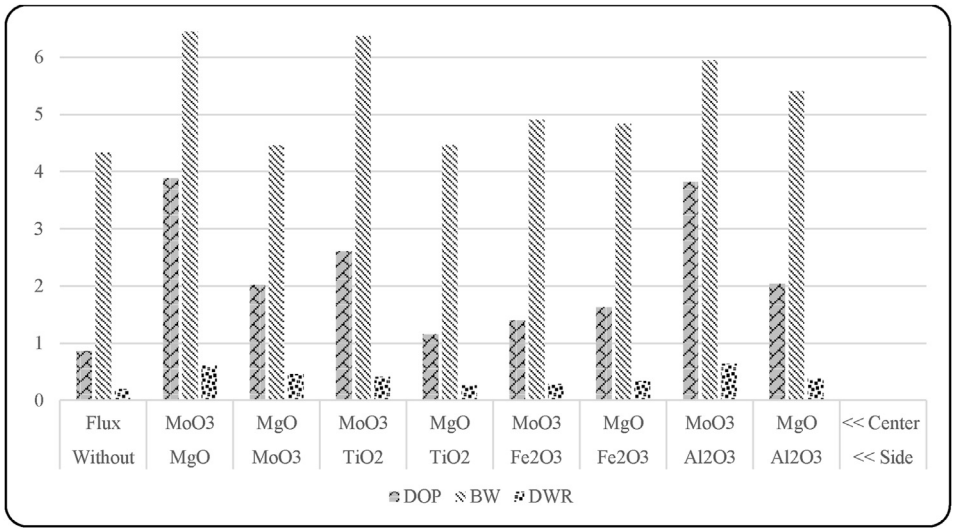

Fig. 10 – Comparison of DOP, BW and DWR of different FZ-TIG weld samples with normal TIG weld sample.

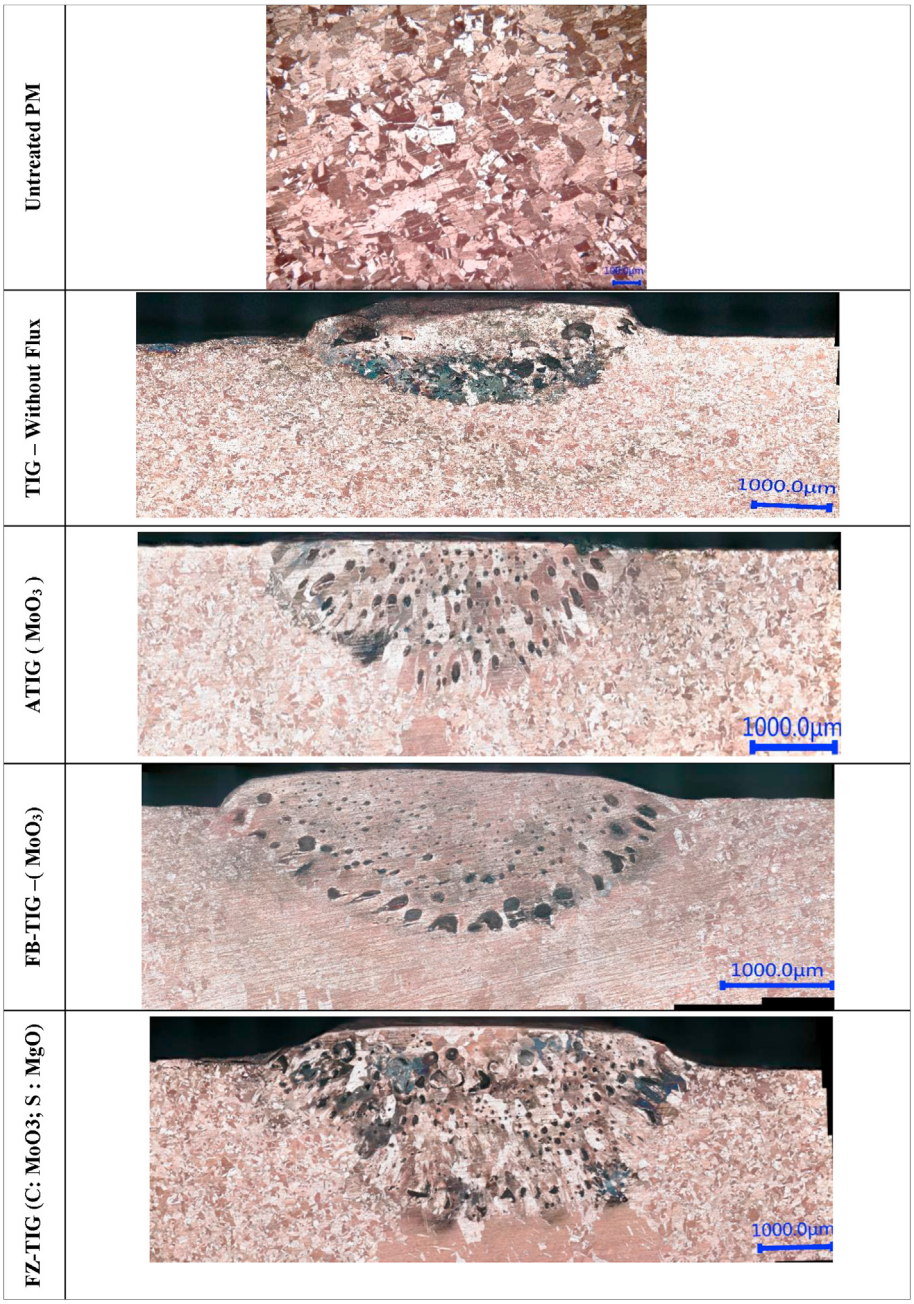

Fig. 11 – Macrostructure of TIG, A-TIG, FB- TIG and FZ- TIG welded samples.

the present set of experiments, the current was kept constant. To withstand uninterrupted arc current (constant current set by welding equipment) arc voltage is required to be increased [42]. To sum up, the existence of arc constriction mechanism may be evidenced by the increase in the peak temperature and arc voltage, which results into the higher DOP and lower weld BW. Nevertheless, there were a few fluxes such as ZnO, MnO_2, and Co_3O_4 which indicated exactly reversed phenomenon. They displayed lower voltage and peak temperature resulting in the lower DOP as compared to the normal TIG samples and rest A-TIG samples.

Moreover, there were the samples such as MnO_2, Co_3O_4, CrO_3, NiO and HgO (reduction respectively in decreasing order) which displayed the higher reduction into the weld width as compared to rest. This phenomenon can be explained by the weld shape model represented by Xu et al. [46] The fluid flow in the weld pool is driven by the combination of the buoyancy force, Lorentz force, and the surface tension. The Marangoni convection balances against the surface tension on the top surface of the weld pool, which is the main driving force of the fluid flow. In the course of the Marangoni convection, the ratio of the surface tension temperature coefficient ($\delta\gamma/\delta T$) majorly enacts the arc forces and weld shape thereby. As per the mechanism, the dissolved flux in the molten weld puddle can change the surface tension (γ) properties while welding. Existing literatures [47,48] suggest that the existing active elements in the weld pool change $\delta\gamma/\delta T$ from negative to positive when the temperature reaches a

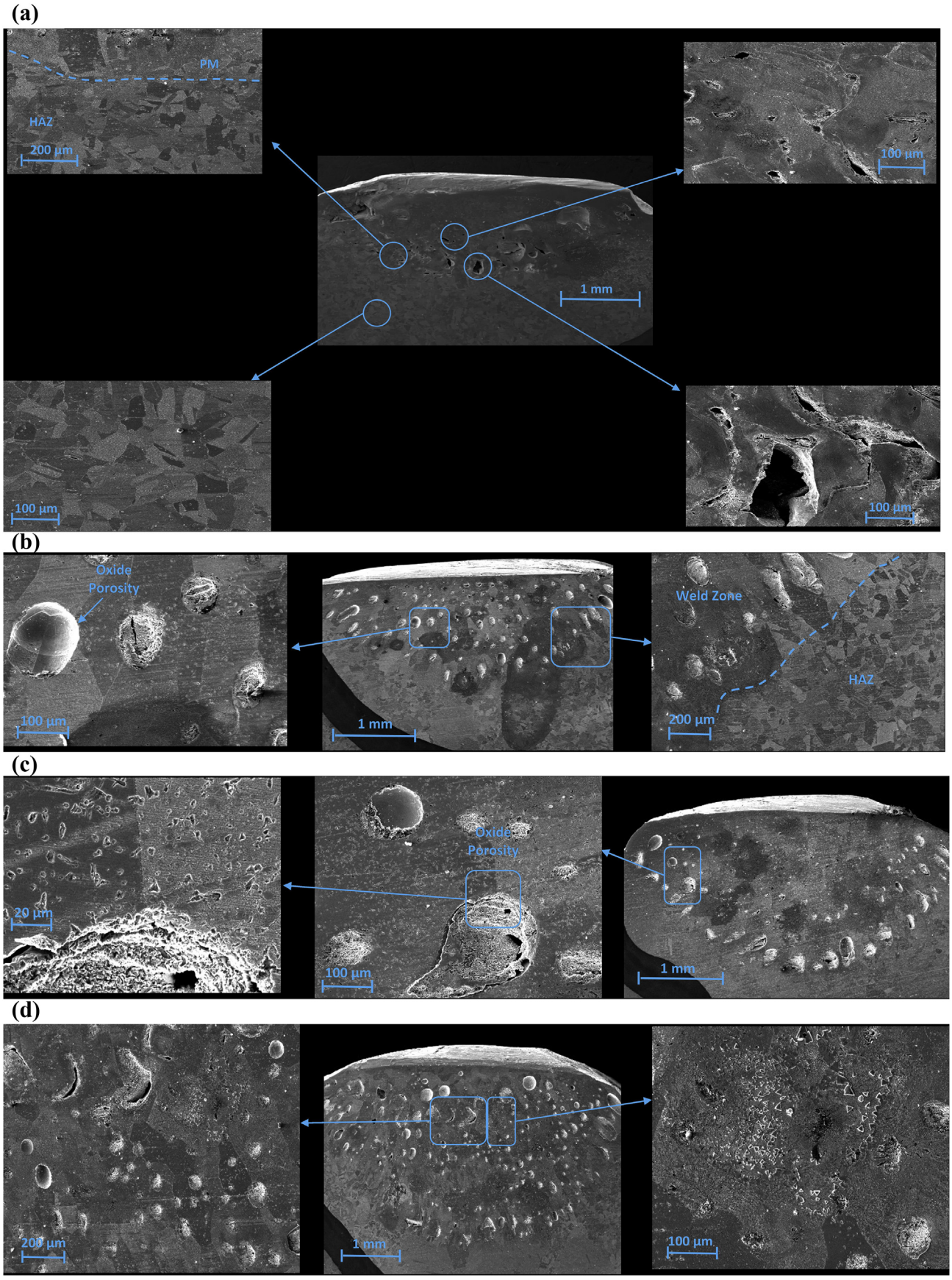

Fig. 12 – SEM micrographs of (a) Normal TIG weld bead (b) A-TIG weld bead with MoO_3 Flux (c) FB-TIG weld bead with MgO Flux (d) FZ-TIG weld bead with Center: MoO_3; Side: MgO Flux.

Table 4 – EDS analysis of the normal TIG welding sample along with specimen exhibiting best DOP in all variants.

	EDS LOCATION	ELEMENTAL GRAPH	Element	Wt%
TIG SPECIMEN	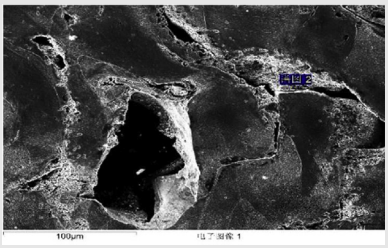	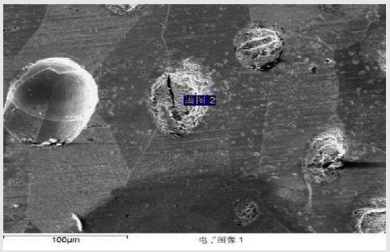	Cu K	100
A-TIG (MoO_3)	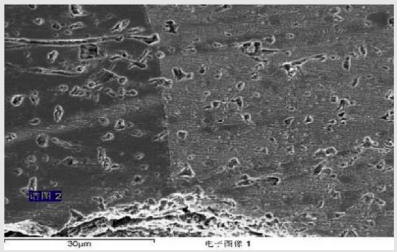	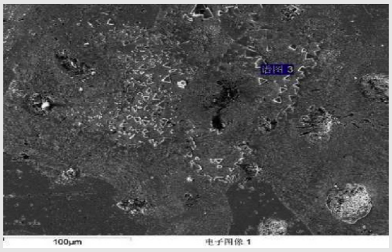	Cu K O K	96.30 03.70
FB-TIG (MoO_3)	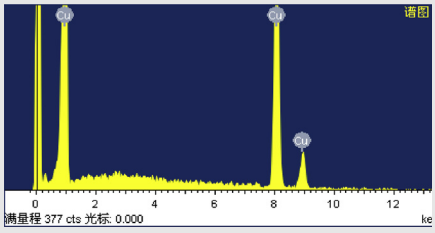	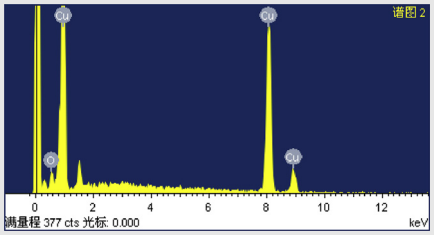	Cu K O K	96.43 03.57
FZ-TIG (C: MoO_3 S: MgO)	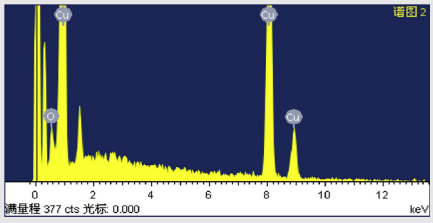	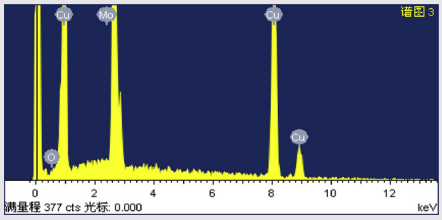	Cu K O K Mo L	97.53 02.47 00.00

certain degree. The Marangoni convection impetuses the molten metal flow radially inward to the weld bead center and resulting into the higher DOP and lower weld BW. However, the negative $\delta\gamma/\delta T$ coefficient makes Marangoni convection drive the metal flow radially outward if the temperature is below this critical value. This phenomenon of the fluid flow makes the weld bead have a high DOP in the center and stretch out on the edge. The results have been witnessed with CaF_2 flux sample. Here, the fluid flow is driven by the buoyancy and Lorentz forces. Conversely, when the temperature crosses the critical value with still negative $\delta\gamma/\delta T$ coefficient, the liquid metal is driven radially inward which results into the reduction in weld width with nominal/no increase in the DOP. However, as the fluxes used in the present study are more thermally insulative as compared to the substrate, the occurrence of the insulation effect is also evident.

Apart from this, several FB-TIG welding samples exhibited higher DOP as compared to TIG welding samples but less than A-TIG samples (Fig. 9). Such outcomes are attributed to the dominant effect of arc constriction and less evident Marangoni convection leading to the deeper weld bead but not the narrow one. Whereas in the case of the A-TIG welding the combined influence of the said effects plays a crucial role in increasing DOP and narrowing down weld bead. The specimens prepared with the MgO and MoO_3 displayed the superior results as compared to the rest owing to the higher oxide disintegration and resulting higher temperature as well as the DOP as described in Section 3.1.

In line to the results achieved with the fluxes delivering higher DOP in the A-TIG and FB-TIG experiments (MoO_3 and MgO) also repeated the favourable outcomes in the FZ-TIG experiments. Marangoni convection, oxide insulation and arc constriction mechanisms acted in conjunction to deliver extra ordinarily higher DOP and DWR as discussed in the rest of the two methods (A-TIG and FB-TIG welding). Hence these outcomes were further justified with the combination of

fluxes which delivered best results for those individual methods (Center: MoO_3; Side: MgO) as displayed in chart (Fig. 10).

3.4. *Effect of fluxes on macrostructures and microstructures*

The typical macrostructures and SEM micrographs of the untreated parent metal (PM) is compared with the TIG, A-TIG, FB-TIG, and FZ-TIG specimens which exhibited highest DOP among aforementioned fluxes and their combinations in Figs. 11 and 12. The microstructure of TIG and A-TIG variants samples comprises of distinct zones viz., fusion zone (FZ), PM and heat affected zone (HAZ) with distinct grain morphology.

The sample without flux exhibited columnar grain in the FZ as shown in Fig. 11. It is worth noting that the samples processed with A-TIG and FZ-TIG demonstrated long needle-shaped grains while those with FB-TIG welding displayed cellular grains in the FZ. That is important because the FZ of A-TIG and FZ-TIG experiences cyclic rapid heating as the weld line being covered by flux leads to the high current density and strong Marangoni convection and arc constriction thereby. Moreover, this rapid heating is followed by rapid cooling owing to high thermal conductivity of the copper instigating directional solidification towards HAZ which hinders the grain growth and make them stretched [49] (see: Fig. 12(b) and (d)). Nonetheless, the scenario in the FB-TIG is altered as the weld line is free from any kind of flux though that present in the side region leads to arc constriction. However, presence of arc constriction generated by side flux but with limited current density almost identical to TIG welding makes the FZ moderately heated followed by slow cooling which allows the grains to grow in the cellular structure as evident in Fig. 12(c). While in the case of TIG welding in absence of any such mechanisms FZ pass through the slow heating and cooling cycle leading to the columnar structure (Fig. 12). Apart from the FZ, the HAZ mainly composed of very fine grain morphology owing to a faster cooling led by heat current towards cold parent metal. That is to say that due to such very hastened thermal cycle the precipitate did not dissolved instigating hindrance to the grain growth and resulting finer grains.

Nevertheless, the microstructural analysis of all aforesaid specimens revealed the defects like porosity and cracks with the varying amount in the FZ. It is worth to notice that the amount of weld porosity generated in descending order could be listed as A-TIG, TIG, FZ-TIG, FB-TIG respectively. This is important because on one hand during the course of A-TIG, FZ- TIG, FB-TIG the porosities were mostly generated on account of the oxygen entrapment while on the other hand during the course of TIG welding it was majorly due to the moisture absorbance. However, highly distinct oxide entrapment mechanism for each A-TIG, FZ-TIG and FB- TIG were evident reportedly. In the course of A-TIG welding, oxygen evolved by decomposition of the oxide-based flux during welding is believed generally to be dissolved into the molten metal which could escape to the environment upon solidification. However, the substrate in the present study is copper, which liberates heat at a stratling rate and hence oxygen molecules are entrapped amid grains and forms porosities. Hence, one may claim that amount of porosity is dependent upon the oxide present in the flux. It has been reported that surface coatings such as ZnO, Fe_2O_3, MoO_3 may generate ample amounts of fume during welding which augments the chances to entrap the evolved gases into the weld [50]. The microstructures and further elemental analysis performed using EDS revealed that use of the oxygen rich fluxes like MoO_3 & Fe_2O_3 resulted into the higher number of porosities as compared to rest which is attributable to the oxygen entrapment leaving voids behind. The EDS analysis of the A-TIG and FZ-TIG sample processed using MoO_3 flux confirmed the presence of such entrapped oxygen in the FZ as depicted in Table 4. However, any sign of Mo inclusion was absent as noticed in the EDS analysis of both the techniques which is attributable to very high arc purging force and elevated peak temperatures thereby. Such tremendous heat leads evaporation of any elemental residue of the flux (Mo) into the atmosphere. Though it is obvious for the A-TIG and FZ-TIG specimens to have oxygen inclusions as the weld line is coated with oxygen rich MoO_3 flux, but FB-TIG specimen EDS analysis revealed such oxygen inclusion as shown in Table 4. It has been published by Fan et al. [51] that many a times during FB-TIG welding the arc is not limited only to the arc span especially when the side flux coat possesses limited electrical resistivity which enforces the inward fluid flow in the surface of welding pool bringing the activating flux particles into the central region. Still such an inward particle flow helps in boosting the weld penetration, simultaneously it also leaves behind the voids generated by the oxygen decomposed off the flux as described earlier in this section.

Alternatively, specimens processed without flux also displayed the porosities and larger voids in the FZ as depicted in Table 4. Therefore, it may be postulated to have multiple causes of the porosity formation during TIG welding. It has been reported that nitrogen and oxygen absorption in the weld puddle generally caused by poor gas shielding [50]. Even 1% air entrainment in the shielding gas may cause distributed porosity while>1.5% results in gross surface breaking pores. Additionally, very often instances like leaks in the gas line, too high a gas flow rate, draughts and excessive turbulence in the weld pool may opt for generation of porosity. One other theory suggested by Lin et al. [52] says that as the temperature surpassed 400 °C during the TIG welding process of pure copper, pores are generated due to the rapid diffusion of hydrogen atoms which had reacted with Cu_2O to produce H_2O. Once the temperature cross over critical temperature of water the cuprous oxide inclusion is substituted by the water steam bubbles. Since the steam is not soluble in copper the steam bubbles exert tremendous pressure on the surrounding metals and voids are left behind upon evaporations.

4. Conclusions

In the present investigation, the influence of several different fluxes on the weld bead dimensions and their microstructures resulted from TIG welding and its different variants were studied in detail. The main results obtained can be summarized as follows:

1. Flux assisted TIG welding of oxygen free copper was successfully carried out applying various fluxes using assorted penetration enhancing techniques like A-TIG, FB-TIG and FZ-TIG. The most effective technique emerged out to be FZ-TIG welding in the pursuit of enhancing weld penetration. The depth of penetration was increased by ~353% for the flux combination of MoO_3 in centre region while MgO in the side region (as compared to conventional TIG welding).
2. A-TIG welding technique delivered maximum penetration using MoO_3 flux which is ~107% more than conventional TIG welded sample which was resulted by Marangoni convection and arc constriction mechanisms. Also, the fluxes like MgO, SiO_2, CaF_2 and $MgCl_2*6H_2O$ showed considerable increase in weld penetration.
3. FB-TIG welding turned out be a least effective technique with 70–75% increase in the weld depth using MgO & MoO_3 fluxes which delivered the superior results in A-TIG welding too.
4. Weld surface appearance of the A-TIG and FZ-TIG variants welded samples were mostly inferior to that of TIG welded samples. Fluxes such as CaO, SiO_2, MoO_3, MgO, NiO exhibited a line of spatter parallel and in the vicinity of the weld bead which may be attributed to strong arc constriction effect and relatively higher peak temperatures. However, spatter-free surfaces were evident during the course of CuO, HgO, CrO_3 fluxes, attributing to the slag layer formed by the flux prior to the welding.
5. Reverse Marangoni mechanism was observed mostly opt with majority of the fluxes in A-TIG (viz., SiO_2, MoO_3, MgO, CaF_2 and $MgCl_2*6H_2O$) and FZ-TIG (except MgO (centre) with TiO_2 and Al_2O_3 (side)) welding techniques considerably raising DOP and D/W ratios.
6. Superior outcomes like higher arc voltage and peak temperatures evidenced in A-TIG welding with fluxes MoO_3, MgO, NiO, HgO, CaF_2 and $MgCl_2*6H_2O$. Whereas MoO_3, MgO and CaF_2 fluxes raised DOP in FB-TIG owing to the strong arc constriction mechanism, in the majority of the FZ-TIG welding specimens both reverse Marangoni and arc constriction played a vital role for the purpose.
7. Microstructural characterization done with a few samples indicated the distinct grain morphology in the different weld zones resulted by distinct welding techniques. While the FZ of the specimens comprised of elongated coarse grains attributable to the faster heating–cooling cycle and directional solidifications, HAZ was occupied by the very fine grain morphologies owing to post weld supercooling.
8. SEM and EDS analysis revealed different amounts of porosities in the FZ and HAZ of distinct specimens. During the course of A-TIG, FZ- TIG, FB-TIG the porosities were mostly generated on account of the oxygen entrapment while in TIG welding it was majorly due to the atmospheric moisture absorbance.

Declaration of Competing Interest

The authors declare that they have no known competing financial interests or personal relationships that could have appeared to influence the work reported in this paper.

Acknowledgment

Authors are grateful to Pandit Deendayal Petroleum University, Gandhinagar, India for providing a platform for conducting experiments and testing. We would like to thank Board of Research In Fusion Science & Technology (BRFST) and Institute for Plasma Research (IPR) Gandhinagar, Gujarat, India (project no Grant Id. NFP-08/MAT/01) for extending financial support.

REFERENCES

[1] Gurevich S, Zamkov V, Kushnirenko N. Improving the penetration of titanium alloys when they are welded by argon tungsten arc process. Automat Weld 1965;18:1–5.
[2] Nayee SG, Badheka VJ. Effect of oxide-based fluxes on mechanical and metallurgical properties of dissimilar activating flux assisted-tungsten inert gas welds. J Manuf Process 2014;16:137–43.
[3] Modenesi PJ, Apolinario ER, Pereira IM. TIG welding with single-component fluxes. J Mater Process Technol 2000;99:260–5.
[4] Zhang R-H, Fan D. Weldability of activating flux in A-TIG welding for mild steel. Han Jie Xue Bao 2003;24:85–7.
[5] Paton B, Lobanov L. Trends in research and developments of the EO Paton Electric Welding Institute in the field of welding and strength of aerospace engineering structures. In: Proc Int Forum on 'Welding technology in aviation and space industries', Beijing, China; 2004. p. 1–7.
[6] Simonik A, AG S. Influence of halides on the penetration effect in argon-arc welding of titanium alloys. 1974.
[7] Howse D, Lucas W. Investigation into arc constriction by active fluxes for tungsten inert gas welding. Sci Technol Weld Join 2000;5:189–93.
[8] Paskell T, Lundin C, Castner H. GTAW flux increases weld joint penetration. Weld J 1997;76:57–62.
[9] Sire S. New perspectives in TIG welding of aluminium through flux application. In: Proceedings of the 7th international symposium, vol. 2001. Japan: Kobe; 2001. p. 113–8.
[10] Lin H-L, Wu T-M. Effects of activating flux on weld bead geometry of Inconel 718 alloy TIG welds. Mater Manuf Process 2012;27:1457–61.
[11] Huang Y, Fan D, Shao F. Alternative current flux zoned tungsten inert gas welding process for aluminium alloys. Sci Technol Weld Join 2012;17:122–7.
[12] Jayakrishnan S, Chakravarthy P. Flux bounded tungsten inert gas welding for enhanced weld performance—a review. J Manuf Process 2017;28:116–30.
[13] Korra NN, Vasudevan M, Balasubramanian K. Optimization of A-TIG welding of duplex stainless steel alloy 2205 based on response surface methodology and experimental validation. Proc IME J Mater Des Appl 2016;230:837–46.
[14] Afolalu SA, Samuel OD, Ikumapayi OM. Development and characterization of nano-flux welding powder from calcined coconut shell ash admixture with FeO particles. J Mater Res Technol 2020;9:9232–41.
[15] Vora JJ, Badheka VJ. Improved penetration with the use of oxide fluxes in activated TIG welding of low activation ferritic/martensitic steel. Trans Indian Inst Met 2016;69:1755–64.
[16] Ramkumar KD, Kumar BM, Krishnan MG, Dev S, Bhalodi AJ, Arivazhagan N, et al. Studies on the weldability,

microstructure and mechanical properties of activated flux TIG weldments of Inconel 718. Mater Sci Eng, A 2015;639:234–44.
[17] Dhandha KH, Badheka VJ. Effect of activating fluxes on weld bead morphology of P91 steel bead-on-plate welds by flux assisted tungsten inert gas welding process. J Manuf Process 2015;17:48–57.
[18] Kumar SA, Sathiya P. Experimental investigation of the A-TIG welding process of Incoloy 800H. Mater Manuf Process 2015;30:1154–9.
[19] Li S, Shen J, Cao Z, Wang L, Xu N. Effects of mix activated fluxes coating on microstructures and mechanical properties of tungsten inert gas welded AZ31 magnesium alloy joints. Sci Technol Weld Join 2012;17:467–75.
[20] Babu AS, Giridharan P, Narayanan PR, Narayana Murty S, Sharma V. Experimental investigations on tensile strength of flux bounded TIG welds of AA2219-T87 aluminum alloy. J Adv Manuf Syst 2014;13:103–12.
[21] Santhana Babu A, Giridharan P, Ramesh Narayanan P, Narayana Murty S. Microstructural investigations on ATIG and FBTIG welding of AA 2219 T87 Aluminum alloy. Appl Mech Mater 2014:489–93. Trans Tech Publ.
[22] Jayakrishnan S, Chakravarthy P, Rijas AM. Effect of flux gap and particle size on the depth of penetration in FBTIG welding of aluminium. Trans Indian Inst Met 2017;70:1329–35.
[23] Zhao Y, Yang G, Yan K, Liu W. Effect on formation of 5083 aluminum alloy of activating flux in FBTIG welding. Adv Mater Res 2011:2385–8. Trans Tech Publ.
[24] Yong H, Feng S, Ding F, Tao L. Flux zoned activating TIG welding of aluminum alloys. Weld Join Harbin 2007;5:47.
[25] Marya M. Theoretical and experimental assessment of chloride effects in the A-TIG welding of magnesium. Weld World 2002;46:7–21.
[26] Gurram M, Adepu K, Pinninti RR, Gankidi MR. Effect of copper and aluminium addition on mechanical properties and corrosion behaviour of AISI 430 ferritic stainless steel gas tungsten arc welds. J Mater Res Technol 2013;2:238–49.
[27] Segletes DS and Amos DR. A-TIG welding of copper alloys for generator components. Google Patents, 2007.
[28] Rana H, Badheka V. Influence of friction stir processing conditions on the manufacturing of Al-Mg-Zn-Cu alloy/boron carbide surface composite. J Mater Process Technol 2018;255:795–807.
[29] Patel P, Rana H, Badheka V, Patel V, Li W. Effect of active heating and cooling on microstructure and mechanical properties of friction stir–welded dissimilar aluminium alloy and titanium butt joints. Weld World 2020;64:365–78.
[30] Huang Y, Meng X, Lv Z, Huang T, Zhang Y, Cao J, et al. Microstructures and mechanical properties of micro friction stir welding (μFSW) of 6061-T4 aluminum alloy. J Mater Res Technol 2019;8:1084–91.
[31] Singh VP, Patel SK, Ranjan A, Kuriachen B. Recent research progress in solid state friction-stir welding of aluminium–magnesium alloys: a critical review. J Mater Res Technol 2020;9:6217–56.
[32] Walker P, Tarn WH. CRC handbook of metal etchants. CRC press; 1990.
[33] Huang H, Shyu S, Tseng K, Chou C. Evaluation of TIG flux welding on the characteristics of stainless steel. Sci Technol Weld Join 2005;10:566–73.
[34] Shyu S, Huang H, Tseng K, Chou C. Study of the performance of stainless steel A-TIG welds. J Mater Eng Perform 2008;17:193–201.
[35] Berthier A, Paillard P, Carin M, Valensi F, Pellerin S. TIG and A-TIG welding experimental investigations and comparison to simulation: Part 1: identification of Marangoni effect. Sci Technol Weld Join 2012;17:609–15.
[36] Lowke J, Tanaka M, Ushio M. Mechanisms giving increased weld depth due to a flux. J Phys D Appl Phys 2005;38:3438.
[37] Kou S. Welding of metallurgy. Kanada: A Wiley Interscience Publication. University of Winconsin; 1987.
[38] Chern T-S, Tseng K-H, Tsai H-L. Study of the characteristics of duplex stainless steel activated tungsten inert gas welds. Mater Des 2011;32:255–63.
[39] Vasantharaja P, Vasudevan M. Optimization of A-TIG welding process parameters for RAFM steel using response surface methodology. Proc IME J Mater Des Appl 2018;232:121–36.
[40] Wu CS. Welding thermal processes and weld pool behaviors. CRC Press; 2011.
[41] Berthier A, Paillard P, Carin M, Pellerin S, Valensi F. TIG and A-TIG welding experimental investigations and comparison with simulation: Part 2–arc constriction and arc temperature. Sci Technol Weld Join 2012;17:616–21.
[42] Tseng K-H, Chen K-L. Comparisons between TiO2-and SiO2-flux assisted TIG welding processes. J Nanosci Nanotechnol 2012;12:6359–67.
[43] Keene B. Review of data for the surface tension of pure metals. Int Mater Rev 1993;38:157–92.
[44] Leconte S, Paillard P, Chapelle P, Henrion G, Saindrenan J. Effect of oxide fluxes on activation mechanisms of tungsten inert gas process. Sci Technol Weld Join 2006;11:389–97.
[45] Fujii H, Sato T, Lu S, Nogi K. Development of an advanced A-TIG (AA-TIG) welding method by control of Marangoni convection. Mater Sci Eng, A 2008;495:296–303.
[46] Xu Y, Dong Z, Wei Y, Yang C. Marangoni convection and weld shape variation in A-TIG welding process. Theor Appl Fract Mech 2007;48:178–86.
[47] Lu S, Fujii H, Nogi K. Marangoni convection and weld shape variations in Ar–O2 and Ar–CO2 shielded GTA welding. Mater Sci Eng 2004;380:290–7.
[48] Fujii H, Lu S, Sato T, Nogi K. Effect of oxygen content in He-O2 shielding gas on weld shape in ultra deep penetration TIG. Trans JWRI 2008;37:19–26.
[49] Lin C-M, Liu J-J, Tsai H-L, Cheng C-M. Evolution of microstructures and mechanical properties of AZ31B magnesium alloy weldment with active oxide fluxes and GTAW process. J Chin Inst Eng 2011;34:1013–23.
[50] Defects/imperfections in welds - porosity. Job Knowledge United Kingdom: TWI Ltd; 2018.
[51] Ding F, Yong H. Study on activating TIG welding for aluminium alloys. Weld World 2005;49/:22–5.
[52] Lin J-W, Chang H-C, Wu M-H. Comparison of mechanical properties of pure copper welded using friction stir welding and tungsten inert gas welding. J Manuf Process 2014;16:296–304.
[53] ChemSpider. Search and share chemistry. Chemical Structure. United Kingdom: Royal Society of Chemistry; 2018.